Atmospheric Research 222 (2019) 154–162

Contents lists available at ScienceDirect

Atmospheric Research

journal homepage: www.elsevier.com/locate/atmosres

What were the changing trends of the seasonal and annual aridity indexes in northwestern China during 1961–2015?

Haihan Zhao[a], Xuebiao Pan[a,*], Ziwen Wang[b,c], Shaojie Jiang[a], Lizhong Liang[a], Xiaochen Wang[a], Xiaoxiao Wang[a]

[a] College of Resources and Environmental Sciences, China Agricultural University, Beijing 100193, China
[b] Qinghai Climate Center, Xining, Qinghai 810001, China
[c] Key Laboratory for Preventing and Mitigating Disaster of Qinghai Province, Xining, Qinghai 810001, China

ARTICLE INFO

Keywords:
Aridity index
Northwestern China
Trend analysis
Seasonal
Climate system indicators

ABSTRACT

The objective of this paper is to study the spatial and temporal variation characteristics of the UNESCO aridity index (AI) at annual and seasonal temporal scales in northwestern China during the 55-year study period (1961–2015). Based on climate data from 178 meteorological stations provided by the China Meteorological Data Service Center, AI trends were investigated by the Mann-Kendall test. The results showed that the annual and seasonal AIs displayed a mixed pattern of positive and negative trends for the period of 1961–2015 across the study area. In most regions, both annual and seasonal AIs exhibited slightly positive trends in northwestern China. Significant ($P < .05$) positive and negative annual trends were detected at 38 and 6 stations, respectively. The highest magnitude of the positive annual trend (0.0037 per year) appeared at Xining station, and the greatest decreasing annual trend (−0.0041 per year) appeared at Minxian station. In terms of seasonal AI, its trend magnitudes varied from −0.0058 to 0.0035 in spring, from −0.0062 to 0.0087 in summer, from −0.0105 to 0.0048 in autumn and from −0.0002 to 0.0443 in winter each year. Our study demonstrated that the AI spatial distribution may tend to be spatially homogeneous in the long term. Abrupt changes varied in different regions and seasons. Nevertheless, the positive trend shifts mostly began in the 1980s and became significant in the following decades. The correlation analysis indicated that the AI in winter and spring was probably mainly affected by the Indian Ocean Warm Pool Strength Index (IOWPSI), while the Multivariate ENSO Index (MEI), the Niño3.4 Sea Surface Temperature Anomaly Index (Niño3.4 SSTA) and the Southern Oscillation Index (SOI) were likely to be the conjoined influencing factors of the AI in summer and autumn. The spatiotemporal features of the long-term AI provided in this study may enhance our scientific understanding of the impacts of recent climate change on dryness/humidity changes in northwestern China; furthermore, this information might potentially be applied in other areas for comparison purposes.

1. Introduction

In past decades, climate changes and human activities have severely influenced the hydrological cycle and have caused series of problems related to water resources (Ma et al., 2008; Yang et al., 2008). Climate change undoubtedly alters the severity of aridity and can cause desiccation in various regions of the world (Cook et al., 2004; Dai, 2011; He et al., 2018). Penck (1910) first proposed that an arid region is where evaporation exceeds precipitation during a certain period. Since then, precipitation (i.e. inflows) and evapotranspiration (i.e., outflows) have been considered as the two main components of the hydrological cycle. Both precipitation and evapotranspiration have strong spatiotemporal variability in their trends and magnitudes (Zarch et al., 2015). In addition, the prevalent understanding is that precipitation is highly variable even at a small scale. Consequently, temporal trends and spatial distribution studies are of great significance for understanding regional scale dryness/humidity change characteristics.

Currently, to assess aridity, the aridity index (AI), defined by the ratio of precipitation (P) to reference evapotranspiration (ET_0) (UNESCO, 1979), is widely adopted in modern climatology. Fu and Feng (2014) referred to the AI as a quantitative indicator of the degree of water vapor deficiency required to meet the evaporation demand at a given location. Under the UNESCO classification, the climate zone was divided into hyper-arid (AI < 0.03), arid (0.03 < AI < 0.2), semi-arid

* Corresponding authors.
E-mail address: panxb@cau.edu.cn (X. Pan).

https://doi.org/10.1016/j.atmosres.2019.02.012
Received 27 June 2018; Received in revised form 17 February 2019; Accepted 20 February 2019
Available online 25 February 2019

(0.2 < AI < 0.5), sub-humid (0.5 < AI < 0.75), and humid (AI > 0.75) regions. In arid zones (i.e., hyper-arid, arid and semi-arid), the study of the AI trends has more significance than that in humid zones (i.e., sub-humid and humid) because minor variations in aridity can easily induce significant changes in arid ecosystems (Schwalm et al., 2017; Yang et al., 2008). The impacts of climate change on aridity have attracted serious concerns in recent decades. An increase in aridity, as the UNESCO AI decreased, was found in some critical agricultural regions, such as in northern and northwestern Iran from 1966 to 2005 (Tabari and Aghajanloo, 2013) and in Turkey for the period of 1930–1993 (Türkes, 2003). Nastos et al. (2013) reported a progressive shift from the humid class towards the sub-humid and semi-arid classes in eastern Greece during 1951–2000. Zarch et al. (2015) concluded that a non-significant aridity trend existed in five-sixths of the world during the period of 1960–2009.

The region of northwestern China is a wide region with a diverse ecological environment, and it appears to be more vulnerable to global changes in climate, with a significant impact on hydrological parameters (Zhai et al., 2005; Shi et al., 2007). Water resources are extremely important and strategic for maintaining regional ecological balance, and water is the key factor that restricts local agricultural production and socio-economic development, especially in the water-stressed areas of northwestern China (Bao and Zou, 2018). Due to the continued population growth, rapid urbanization and increasing need for water in agricultural production, it is urgent to acquire a more in-depth understanding of how climate change affects aridity in northwestern China, and this information is useful for scientists and policy-makers. Through the application of the Mann-Kendall (MK) test, it has been reported that precipitation has shown an increasing trend, while ET_0 has shown a decreasing trend in many areas of northwestern China. For example, Yang et al. (2017) investigated the spatiotemporal variations in precipitation across some regions in northwestern China and found that significant increasing trends occurred, especially in the months of January and July. In the Xinjiang Aksu River Basin, Zhang et al. (2015) showed significant increasing trends in the July and October streamflow and in the December precipitation. Zhao et al. (2014) reported that annual ET_0 decreased in eastern Qinghai during 1961–2012. Additionally, based on the observational facts of increasing glacial melt water, river runoff and water level of inland lakes, Shi et al. (2007) hypothesized that a climatic shift from a warm-dry to a warm-humid pattern occurred in northwestern China in the 1970s.

Various methods or models are available and have been used to estimate aridity in previous studies of northwestern China, but the results of these methods or models are inconsistent (Wang et al., 2014; Huo et al., 2013; Liu et al., 2013) due to their different definitions and input data requirements. Therefore, it is very difficult to compare the degree of aridity globally. As a result, our study used the UNESCO AI due to its quantitative classification of climate zones and wide global application. Furthermore, our study is based on a much wider geographical scale (6 provinces) and temporal scale (1961–2015) and attempts to strengthen temporal trend analysis by applying more appropriate nonparametric tests at both annual and seasonal scales. The present study aims to (1) reveal long-term (1961–2015) temporal and spatial variations in the AI time series from 178 meteorological stations at seasonal and annual time scales by applying the MK method and the Theil-Sen approach (TSA); (2) detect temporal trend shifts using the Sequential Mann-Kendall (SQMK) method; and (3) analyze the relationships between the AI and nine possible influential climate system indicators. It is expected that the findings of this paper will provide a scientific basis for the comprehensive assessment of aridity and the effective management of limited water resources, thus contributing to mitigating the adverse influences of climate change on hydrology and agricultural production and improving the regional ecological environment.

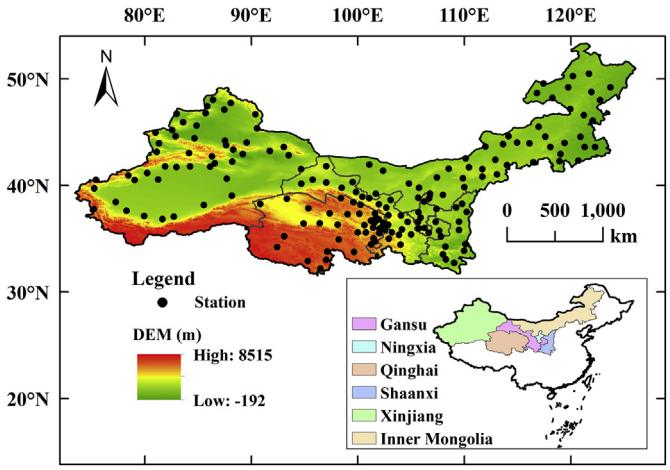

Fig. 1. Study area and meteorological stations.

2. Materials and methods

2.1. Study area and data description

In this study, the following provinces were included: Shaanxi, Gansu, Qinghai, Ningxia, Xinjiang, and Inner Mongolia, which encompassed a total area of 4.6 million km^2 (31–54°N, 73–127°E) (Fig. 1); this value approach one-half of the land area of China. Inner Mongolia (37–54°N, 97–127°E) is not a northwestern province in terms of traditional administration definitions, but as a transition zone between the eastern humid and semi-humid regions and the western arid and semi-arid inland regions, it is important to include it in aridity analysis. From east to west, the study area extends into the Eurasian continent. Due to the effect of the Tibetan Plateau terrain and the high mountain barriers, such as the Tianshan Mountains, Kunlun Mountains and Qilian Mountains, it is difficult for moist air currents to reach the area (Shi et al., 2007). As a result, the arid and semi-arid inland region in northwestern China has a typical continental climate with a low annual precipitation, wide temperature range and high evaporation (Deng et al., 2014). It is a region with severe water scarcity, in which the regional ecosystems are highly vulnerable under the effects of global warming (Yang et al., 2008).

The daily time series of sunshine duration, temperature (maximum and minimum temperature), relative humidity and wind speed for 178 meteorological stations distributed in the study area (Fig. 1) were obtained from 1961 to 2015 from the China Meteorological Data Service Center (CMDC) (http://data.cma.cn/). Strict quality and homogenization control tests were conducted by the National Meteorological Information Center (NMIC) before the data were released. Missing data were further screened according to the method applied by Hu et al. (2015). We defined spring as March, April and May; summer as June, July and August; autumn as September, October and November; and winter as December, January and February. Both annual and seasonal meteorological data were computed by daily data. Additionally, the Arctic Oscillation (AO), Multivariate ENSO Index (MEI), Niño3.4 Sea Surface Temperature Anomaly Index (Niño3.4 SSTA), North Atlantic Oscillation (NAO), Pacific Decadal Oscillation (PDO), Quasi-Biennial Oscillation (QBO), Southern Oscillation Index (SOI) and Western Hemisphere Warm (WHWP) were made available by the Earth System Research Laboratory (https://www.esrl.noaa.gov/psd/data/climateindices). The Indian Ocean Warm Pool Strength Index (IOWPSI) was obtained from the National Climatic Center (NCC) (http://cmdp.ncc-cma.net/cn/monitoring.htm) of the China Meteorological Administration (CMA). We calculated the annual and seasonal climate system indicators by taking the 12-month average value in a specific year and the 3-month average value in a specific season.

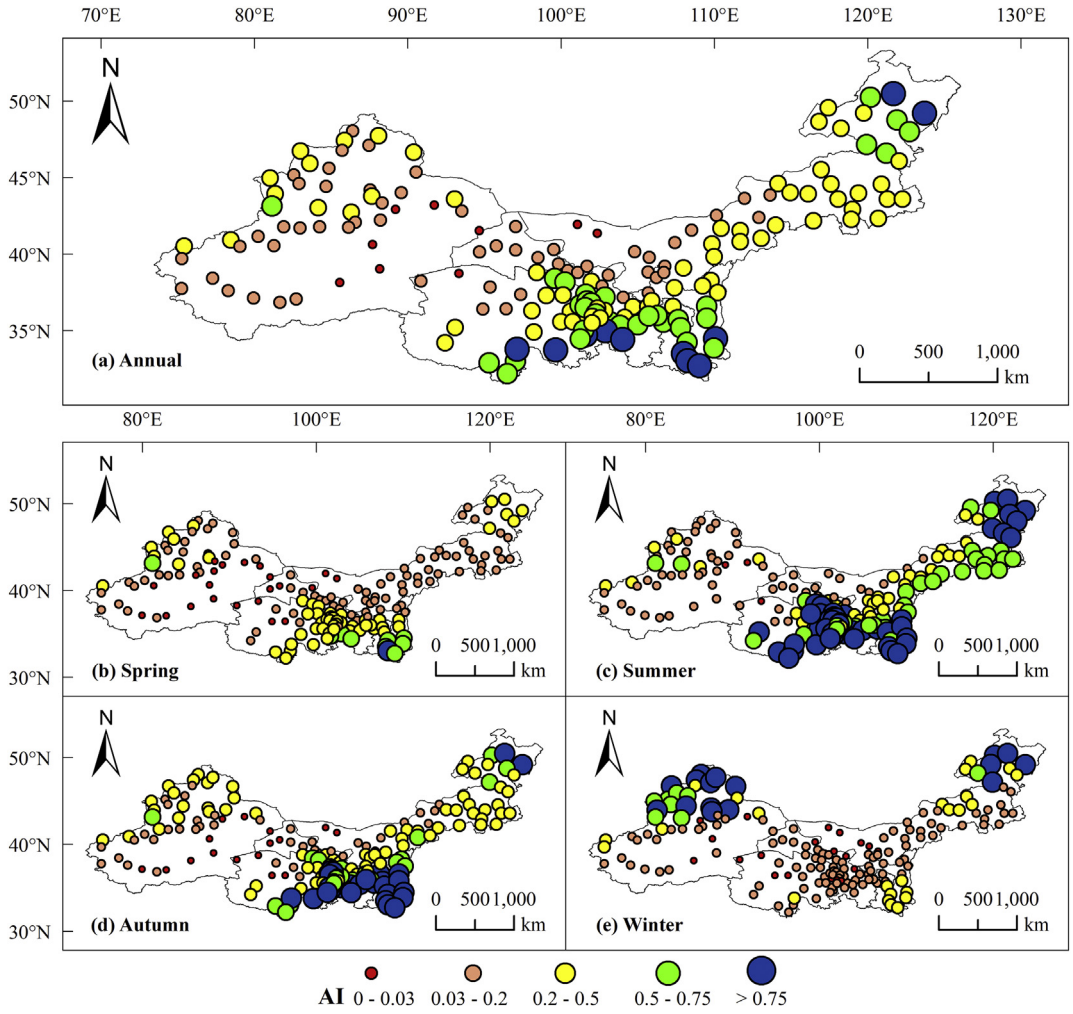

Fig. 2. Spatial distributions of stations with the mean values of the annual and seasonal AI time series from 1961 to 2015.

2.2. Methods

2.2.1. Aridity index

The aridity index is calculated by UNESCO (1979) as:

$$\mathrm{AI} = P/\mathrm{ET}_0 \tag{1}$$

where P is the annual and seasonal total precipitation (mm), and ET_0 is the annual and seasonal total potential evapotranspiration (mm). The annual and seasonal values of precipitation and ET_0 were obtained by adding up the daily values. The Penman–Monteith equation of daily reference evapotranspiration ET_0 (mm), which is recommended by the FAO (Allen et al., 1998), can be expressed as:

$$\mathrm{ET}_0 = \frac{0.408\Delta(R_n\text{-}G) + \gamma\frac{900}{T+273}u_2(e_S\text{-}e_a)}{\Delta + \gamma(1 + 0.34u_2)} \tag{2}$$

where R_n is the net radiation at the crop surface (MJ/(m^2·d)), G is the soil heat flux density (MJ/(m^2·d)), T is the air temperature at a height of 2 m (°C), u_2 is the wind speed at a height of 2 m (m/s), e_S is the vapor pressure of the air at saturation (kPa), e_a is the actual vapor pressure (kPa), Δ is the slope of the vapor pressure curve (kPa/°C) and γ is the psychrometric constant (kPa/°C). The computation of each term required for Eq. (2) followed the methods given by Allen et al. (1998).

2.2.2. Serial correlation effect

Both the MK test and the TSA require time series to be serially independent (von Storch, 1995; Hamed and Rao, 1998). The existence of serial correlation could lead to a rejection of the null hypothesis of no trend by increasing the probability of a significant trend, while the null hypothesis might be true, particularly if the sample size and the magnitude of the trend are both small (Yue et al., 2002; Yue and Wang, 2002). Therefore, the following procedure applied by Yang et al. (2017) was used to remove the influence of possible serial correlation in the time series of the AI (x_1, x_2, …, x_n) before applying the MK test and the TSA.

(1) Compute the lag-1 serial correlation coefficient (r_1) of the AI series, as shown in Eq. (3) (Salas et al., 1980):

$$r_1 = \left[\frac{1}{n-1}\sum_{i=1}^{n-1}(x_i - \bar{x})(x_{i+1} - \bar{x})\right] \Big/ \left[\frac{1}{n}\sum_{i=1}^{n}(x_i - \bar{x})^2\right] \tag{3}$$

where r_1, n, x_i, and $\bar{x}$ are the correlation coefficient lag-1, the sample length, the ith AI value and the mean value of the AI time series, respectively.

(2) For the two-tailed test, the alternative hypothesis is that the true r_1 is different from zero, which indicates that the time series is autocorrelated. According to Salas et al. (1980) and Zhang et al. (2015), the confidence interval of r_1 at the 0.05 significance level is as follows:

$$\frac{-1 - 1.96\sqrt{n-1}}{n-1} \le r_1 \le \frac{-1 + 1.96\sqrt{n-1}}{n-1} \tag{4}$$

(3) If r_1 lies inside the above interval, then the time series is

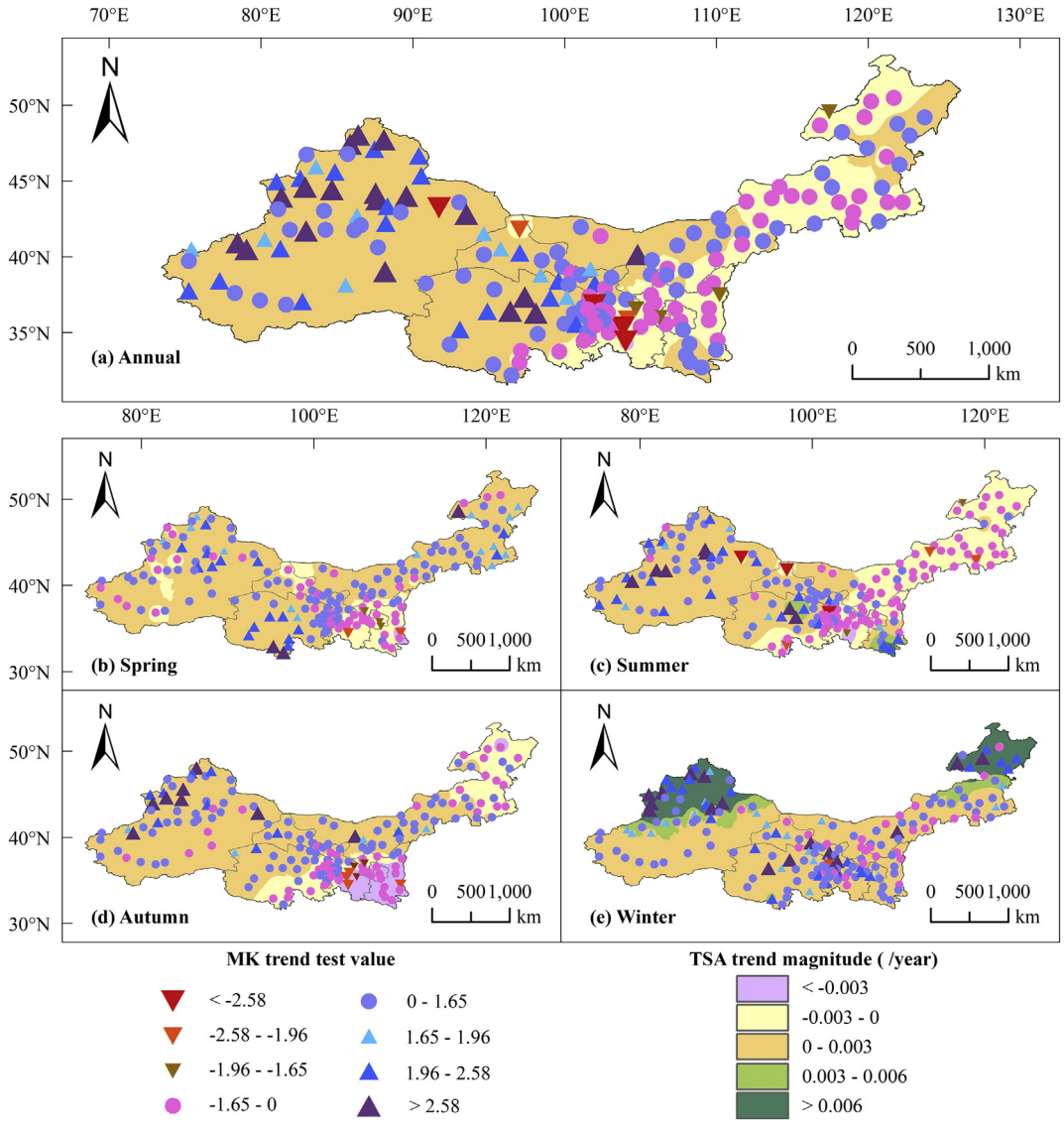

Fig. 3. Spatial distributions of stations with MK statistics and interpolated trend (/year) results from the TSA of annual and seasonal AI time series from 1961 to 2015.

independent, and the MK test and the TSA can be applied directly. In cases where r_1 is outside the above interval, the time series is serially correlated. The autocorrelation may be removed by adopting (x_2-r_1x_1, x_3-r_1x_2, …, x_n-r_1x_{n-1}) as the 'pre-whitened' series (Gocic and Trajkovic, 2013; Sayemuzzaman and Jha, 2014).

2.2.3. Detection of trends

It was suggested by Goossens and Berger (1986) that the nonparametric MK test (Mann, 1945; Kendall, 1975) is the most appropriate method for analyzing changes in climate data series. Parametric trend tests require data to be normally distributed, while non-parametric trend tests do not require prior knowledge of the distribution (Gocic and Trajkovic, 2013). The MK test was performed to evaluate trends in the AI time series, and the TSA was used to calculate the magnitudes of the trends. The MK test statistic S is defined as follows:

$$S = \sum_{i=1}^{n-1} \sum_{j=i+1}^{n} \mathrm{sgn}(x_j - x_i) \tag{5}$$

where sgn (x_j-x_i) is the sign function, which has values equal to −1, 0 and 1 when the argument is negative, zero and positive, respectively. When $n \geq 8$, the statistic S approaches a normal distribution with a mean of zero, and the variance is given in Eq. (6):

$$Var(S) = \left[n(n-1)(2n+5) - \sum_{k=1}^{m} t_k(t_k-1)(2t_k+5) \right] /18 \tag{6}$$

where t_k is the number of ties of extent k, and m is the number of tied values. The MK test statistic Z can be computed by Eq. (7):

$$Z = \begin{cases} (S-1)/\sqrt{Var(S)}, & \text{if } S > 0 \\ 0, & \text{if } S = 0 \\ (S+1)/\sqrt{Var(S)}, & \text{if } S < 0 \end{cases} \tag{7}$$

Positive values of Z indicate positive trends, which means that aridity decreases, while negative values of Z indicate negative trends, i.e., increases in aridity. The null hypothesis of no trend is rejected if $|Z| > Z_{1-\alpha/2}$, where $Z_{1-\alpha/2}$ is the standard normal deviates. At the 5% and 1% significance levels, $Z_{1-\alpha/2}$ is equal to 1.96 and 2.576, respectively.

In addition, Sen's slope (Q_k) of TSA (Theil, 1950; Sen, 1968) can be computed by Eq. (8):

$$Q_k = (x_j - x_i)/(j-i) \text{ for } k = 1, \ldots, N \tag{8}$$

where x_j and x_k are the data values at times j and i ($n > j > i > 1$), respectively, and N is the number of all combinations of recorded pairs in the entire data sample. The median of the total N values of Q_k is Sen's

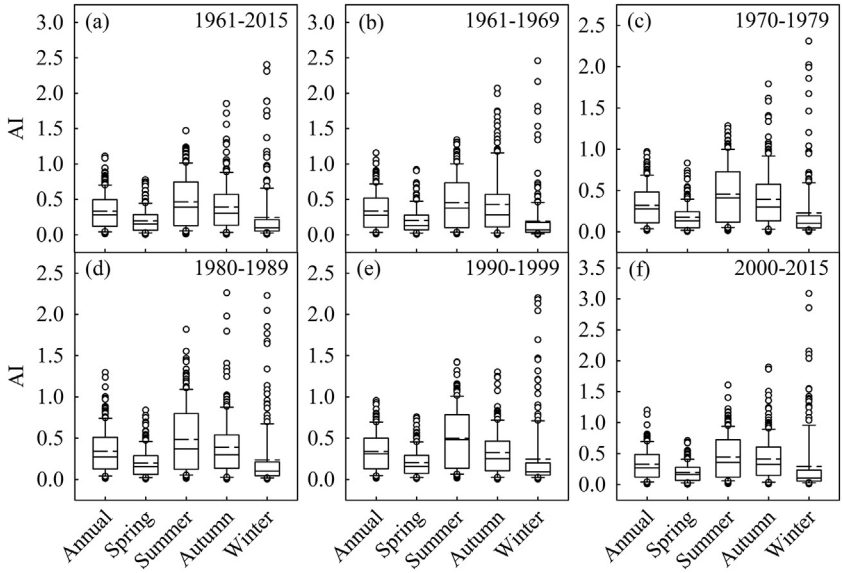

Fig. 4. Box-whisker plots of the inter-decadal and seasonal AI time series of 178 stations. Each plot shows the median (solid line in the box), mean (dashed line), interquartile range (box) and outer quartiles (whiskers).

Table 1
Detailed information of the MK trend test and SQMK results for annual and seasonal AIs.

Time scale	Station	Ab	Longitude (°E)	Latitude (°N)	Altitude (m)	Z	Change year
Annual	Minxian	MX	104.02	34.43	2315.0	−3.01	1990
	Yining	YN	81.33	43.95	662.5	2.92	1984
	Dabancheng	DBC	88.32	43.35	1103.5	2.06	1987
	Qarkilik	QK	88.17	39.03	887.7	3.06	1980
Spring	Xin Barag Right Banner	XBRB	116.82	48.67	554.2	2.60	1975
	Golmud	GM	94.90	36.42	2807.6	2.37	2000
	Huashan	HS	110.08	34.48	2064.9	−2.31	1980
	Kumishi	KMS	88.22	42.23	922.4	2.00	1986
Summer	Ongniud Bannar	OB	119.02	42.93	634.3	−2.19	2003
	Huzhu	HZ	101.95	36.82	2480	−2.73	1982
	Qitai	QT	89.57	44.02	793.5	2.50	1985
	Minfeng	MF	82.72	37.07	1409.5	2.44	1982
Autumn	Anxi	AX	95.77	40.53	1170.9	2.24	1970
	Lintao	LT	103.85	35.35	1893.8	−2.21	1969
	Bayinmaodao	BYMD	104.80	40.17	1323.9	2.79	2002
	Wusu	WS	84.67	44.43	478.7	3.70	1982
Winter	Gaotai	GT	99.83	39.37	1332.2	3.19	1996
	Xiao'ergou	XEG	123.72	49.20	286.1	2.22	1989
	Baotou	BT	109.85	40.67	1067.2	2.61	1979
	Dabancheng	DBC	88.32	43.35	1103.5	3.03	1995

slope estimator (Q_{med}). If N is odd, then $Q_{med} = Q_{(N+1)/2}$, and if N is even, then $Q_{med} = [Q_{N/2} + Q_{(N+2)/2}]/2$. Its value indicates the magnitude of the trend. Finally, the results of the MK test and TSA were mapped using ArcGis 10.2 software.

We performed the SQMK test to identify significant shifts in the AI trends (Sneyers, 1990; Some'e et al., 2012). First, we compared x_j ($j = 1, 2, \ldots, n$) to x_i ($i = 1, 2, \ldots, n-1$) and then counted the numbers (indicated by n_j) of cases where $x_j > x_i$. The sequential progressive value is calculated as follows:

$$t_j = \sum_{1}^{j} n_j \tag{9}$$

$$E(t) = [n(n-1)]/4 \tag{10}$$

$$Var(t_j) = j(j-1)(2j+5)/72 \tag{11}$$

$$UF(t) = [t_j - E(t)]/\sqrt{Var(t_j)} \tag{12}$$

Similarly, the sequential retrograde ($UB(t)$) value is calculated starting from the end of the time series data. The intersection of the UF (t) and $UB(t)$ curves shows the transition point of the trend.

3. Results and discussion

3.1. Spatial distributions of annual and seasonal AIs

The mean values of the annual and seasonal AI time series during the study period are illustrated in Fig. 2. The spatial distribution pattern of the AI presented a reducing trend from the western and eastern regions to the central region (approximately between 80° and 105°E and the regions north of 40°N) of the study area at all time scales. The proportion of meteorological stations with AI values > 0.75 accounted for 6% (annual), 1% (spring), 25% (summer), 16% (autumn) and 9% (winter). Most of these stations are distributed in northeastern Inner Mongolia, southeastern Qinghai, Gansu and Shaanxi and the northern part of Xinjiang (in winter). Notably, the winter climate in Xinjiang is more humid than that in the other seasons (Fig. 2e). This difference is mainly due to a combination of the abundant winter precipitation as a result of westerlies and the Tianshan terrain and ocean influence (Yao

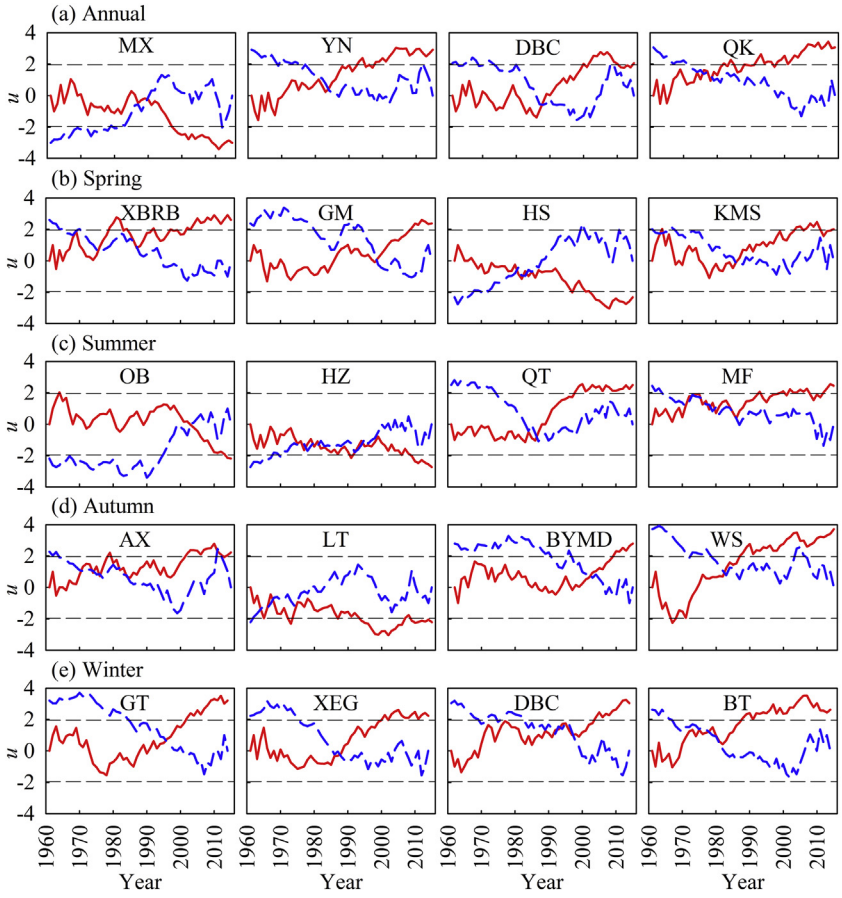

Fig. 5. SQMK analyses for annual and seasonal AIs of the stations based on the MK statistics at the 0.05 significance level. The red solid lines and blue dashed lines represent the progressive series, UF, and the retrograde series, UB. The horizontal dashed lines are the significance level at 0.05. (For interpretation of the references to colour in this figure legend, the reader is referred to the web version of this article.)

et al., 2015). The stations (5% in annual, 12% in spring, 2% in summer, 9% in autumn and 11% in winter) that appear in the hyper-arid class (AI < 0.03) are mainly located in the two largest desert areas of China (i.e., the Taklimakan Desert and the Badain Jaran Desert).The strong seasonal Asian monsoon regime is able to reach the margins of the desert and provides warm and moist currents from July to September, while cold and dry continental air masses frequently influence the area in winter and spring (Li et al., 2016). In general, the AI showed a slightly seasonal change over the study area. In spring, the AI was lower than 0.20, while the AI was close to 0.50 in summer. Lower AI values appear in spring, indicating a high possibility of spring drought, which will have adverse effects on the production of agriculture at the sowing and emergence stages and on animal husbandry during the pasture reviving period.

3.2. Variations in annual and seasonal AIs

3.2.1. Distribution of annual and seasonal AI time series trends

Fig. 3 compares the trends of the AI time series at annual and seasonal temporal scales. For the trend of period of 1961–2015, the AI exhibited a mixture of positive and negative trends at all scales. At the annual scale (Fig. 3a), two-thirds of the stations (117 of 178 stations) displayed positive AI trends, while the remaining stations (61 of 178 stations) had negative trends. It is interesting to note that a higher percentage (73%) of stations in the arid class (hyper-arid, arid and semi-arid) displayed positive trends, while 56% of stations in the humid class (sub-humid and humid) exhibited negative trends. The 38 stations with statistically significant positive trends at the 0.05 level were mostly identified in the western part of the study area, and only 6 stations with significant negative trends were distributed around Gansu, Qinghai and Xinjiang. The highest magnitude of the positive trend (0.0037 per year) appeared at Xining station (36°21′N, 101°45′E), while the most severe decreasing trend (−0.0041 per year) was found at Minxian station (34°26′N, 104°01′E).

Seasonally, the AI time series presented different distribution trend patterns. A large number of stations with positive trends were detected in spring (125 of 178 stations), autumn (113 of 178 stations) and winter (148 of 178 stations) (Fig. 3b, d, e, respectively). Only 19, 17 and 41 stations had significant ($P < .05$) positive trends in spring, autumn and winter, respectively. Most of these stations were found in northern Xinjiang and the southern part of Qinghai in spring. The stations (2 in spring, 4 in autumn, 1 in winter, respectively) in Ningxia, Shaanxi and the southern part Gansu showed significant ($P < .05$) negative trends. In summer, 93 stations showed positive trends in the AI series, with 25 stations being significant; furthermore, 6 out of 85 stations showed significant ($P < .05$) negative trends (Fig. 3c). Meanwhile, an overall majority of stations in the arid class exhibited positive trends (73% in spring, 71% in summer, 79% in autumn and 82% in winter). The higher percentage of hyper-arid, arid and semi-arid stations with positive trends indicated that they were becoming more humid. Moreover, humid (sub-humid and humid) stations were more likely to show negative trends as aridity increased at multiple time scales (e.g., 80% in spring, 71% in summer and 75% in autumn). This result suggests that the AI spatial distribution in the study area tended to be homogeneous over the long term. A consistent pattern was shown in the study by Zarch et al. (2015), which suggested that globally, arid zones were becoming more humid, and humid zones were becoming slightly more arid. In general, the magnitudes of all seasonal AI trends varied from −0.0058 to 0.0035 in spring, from −0.0062 to 0.0087 in summer, from −0.0105 to 0.0048 in autumn and from −0.0002 to 0.0443 in winter each year, and significant positive trends were more prevalent than negative trends in the seasonal AI series.

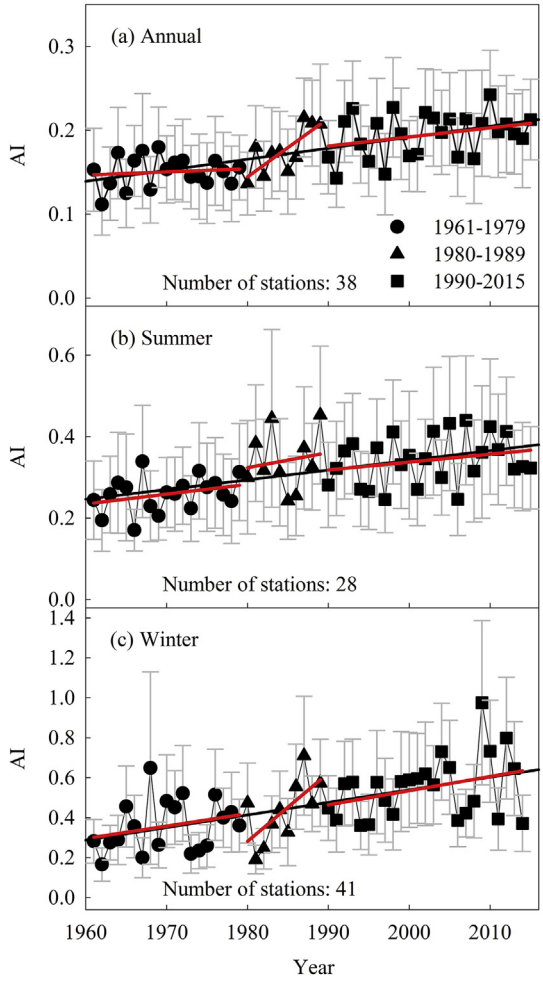

Fig. 6. Time series of annual and seasonal AIs based on data from 1961 to 2015 averaged over the significant increasing trends. The black and red lines represent linear regressions for the period of 1961–2015 and the three sub-periods, respectively. The error bars are the 95% confidence intervals. (For interpretation of the references to colour in this figure legend, the reader is referred to the web version of this article.)

3.2.2. Analysis of inter-decadal and seasonal AI time series

To further investigate variations in the AI over the study area in 1961–2015, the inter-decadal and seasonal AIs were calculated for each station, and the results are shown in Fig. 4. The highest median value of the annual AI appeared in the 1990s (0.31) with the rest of the decades showing between 0.27 and 0.28 (Fig. 4a). Previous studies (Zarch et al., 2015; Liu et al., 2013) have concluded that *P* is a more dominant factor in aridity than in ET_0 in arid regions where the interannual ET_0 does not fluctuate much, and thus, aridity fluctuates only as a result of precipitation variations. From the 1980s to the 1990s, the water cycle was enhanced and accelerated by notable global warming, which led to an increase in precipitation from 30° to 55°N, especially in North America, western Russia and central Asia (Salinger, 2005). Precipitation increased considerably in the western part of northwestern China in the 1990s (Shi et al., 2007). For example, the precipitation in Xinjiang increased by 20%–50% in the 1990s compared to the values measured in the 1980s (Hu et al., 2002). However, after 2000, the increasing rate of precipitation in northwestern China was diminished (Chen et al., 2015). Additionally, increases in air temperature, wind speed and solar radiation have dominated the increase in ET_0 since the mid-1990s (Liu et al., 2013). It may, therefore, be construed that these comprehensive factors explain why the climate of the study area tended to be more humid in the 1990s than in the other decades.

The spring median AI (Fig. 4b) showed an increasing trend that increased rapidly in the 1980s (0.16) from the 1960s and 1970s (0.13). The summer and autumn AIs (Fig. 4c and d, respectively) have exhibited great volatility in recent decades. In summer, the highest median value of 0.48 appeared in the 1990s, and the lowest value of 0.36 was measured in the 2000s. In contrast, the highest and lowest values of AI in autumn appeared in the 2000s and 1990s, respectively. This result suggests that dryness/humidity climatic changes in summer and autumn have been more sensitive to warming in recent decades. The winter AI (Fig. 4e) indicated an increasing trend that was low in the 1960s and high in the 2000s, which was consistent with the observed spring change, over the study area. Additionally, the AI in winter presented great heterogeneity in different decades. Stations with outliers are primarily located in northern Xinjiang and northwestern Inner Mongolia (e.g., Ergun Right Banner, Hailar, Caijiahu, and Yining), which may be closely related to the high frequency of extreme precipitation caused by cold air activity and low evaporation in the cold season (Zhang et al., 2012; Shi et al., 2018; Xin et al., 2009).

3.2.3. Shift analysis of annual and seasonal AIs

For the time series with a significant trend at the 0.05 significance level (i.e., MK test, Z values > 1.96), the SQMK test was applied to analyze the abrupt changes in the AI time series. Table 1 exhibits four cases with a significant trend ($P < .05$) at each timescale, and the results are graphically presented in Fig. 5. The results provide information about the specific station and its surroundings. For YN (annul AI = 0.3), DBC (annual AI = 0.05) and QK (annual AI = 0.02), the starting points of the annual AI series increasing trends occurred in the 1980s, and the trend shifts typically became significant in the subsequent decade. The result at the YN station is consistent with those of previous research (Huo et al., 2013). All three stations are located in Xinjiang and are characterized by an arid climate. These results agree with those of previous studies that revealed a significant abrupt climate change in the mid-1980s in the arid region of northwestern China (Chen et al., 2006). For MX, which is a humid station (annual AI = 0.79) situated in southern Gansu, there was a decreasing trend shift that began in 1990 and became significant around 1996. This increase in aridity was mainly caused by the decreasing trend of annual precipitation, which was the result of the decrease of heavy precipitation events (> 13.6 mm/day) in southern Gansu in autumn (Han et al., 2016). For the seasonal AI time series, the shifts in the increasing trends primarily began in the 1980s and reached significance in the 21st century. Similar

Table 2
Pearson's correlation coefficients between the AI and climate system indicators that may affect the AI in northwestern China during 1961–2015.

	AO	IOWPSI	MEI	Niño3.4 SSTA	NAO	PDO	QBO	SOI	WHWP
Spring	0.28*	0.45***	0.31*	0.29*	0.17	0.04	−0.04	−0.17	0.33*
Summer	0.32*	0.00	−0.12	−0.27*	0.20	0.22	−0.19	0.27*	−0.06
Autumn	0.25	−0.13	−0.45***	−0.43***	0.24	−0.33*	0.08	0.36**	−0.05
Winter	−0.01	0.48***	0.17	0.17	−0.14	0.13	−0.01	−0.10	0.21

* Significant at $P < .05$.
** Significant at $P < .01$.
*** Significant at $P < .001$.

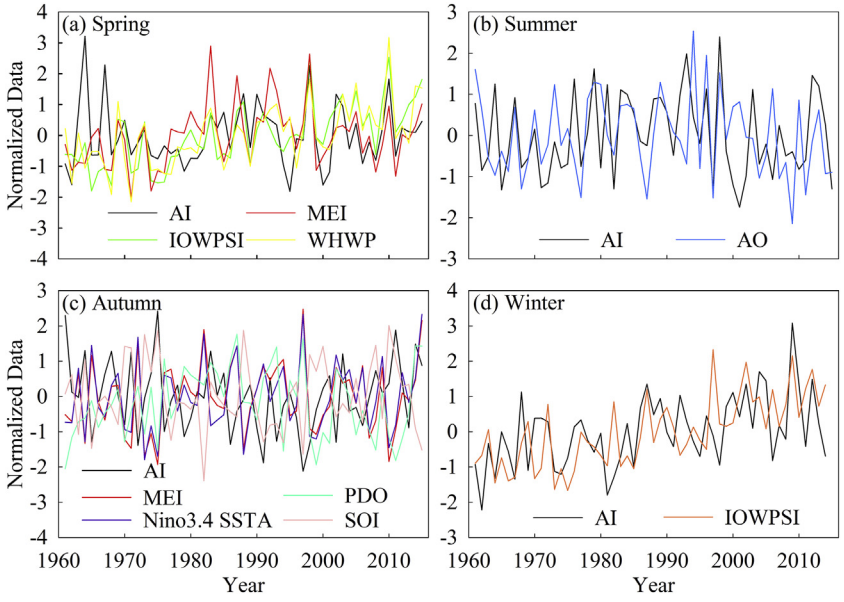

Fig. 7. Seasonal AI and certain climate indicators during 1961–2015.

variation patterns of seasonal dryness/humidity climate have been found on the Tibetan Plateau (Huang et al., 2011; Wang et al., 2014). However, the change points of the decreasing trends varied between stations and between seasons, although the trend shifts normally became significant around the year 2000.

Because positive trends are more dominant in significant trends at all time scales and their transition points were mostly in the 1980s, the study period was split into three sub-periods for further comparison of the changes of significant positive AI trends in northwestern China: 1961–1979 (Period 1), 1980–1989 (Period 2), 1990–2015 (Period 3) (Fig. 6). Summer and winter AIs were used to represent seasonal AIs. Linear regressions showed that the slopes of trends within Periods 1 and 3 were both almost equivalent to the slope of the trend within the entire study period (1961–2015) at each time scale. However, the annual and winter AI trends within Period 2 exhibited a rapid increasing tendency. Additionally, the results of two-sample t-test indicated a significant increase ($P < .01$) in the average AI from Period 1 to Period 3 at the annual and seasonal scales, further suggesting that there was an abrupt change in the 1980s.

3.3. Possible influential climate system indicators of AI variations

Water vapor in northwestern China mainly originates in the Atlantic Ocean, the Arctic Ocean, the Pacific Ocean and the Indian Ocean. Therefore, nine climate system indicators that may affect the dryness/humidity in northwestern China were selected based on previous studies (Li et al., 2016; Yang et al., 2017; Wang et al., 2014), and their relationships with the AI were explored (Table 2). Correlations between the AI and climate system indicators suggest that the dominant factors changed with the season. In spring, the correlation for the AI with IOWPSI ($r = 0.45$, $P < .001$) was higher than those with other factors. In addition, significant correlations ($P < .05$) appeared between the AI and AO, MEI, Niño3.4 SSTA and WHWP. In summer, the AI had a significant correlation ($P < .05$) with AO, SOI and Niño3.4 SSTA. In autumn, MEI ($r = -0.45$, $P < .001$) and Niño3.4 SSTA ($r = -0.43$, $P < .001$) had more significant correlations with AI than the other indicators. Additionally, PDO and SOI had significant correlations ($P < .05$) with the AI. In winter, only IOWPSI was significantly correlated ($r = 0.48$, $P < .001$) with the AI. Taken together, these results suggest that the AI in northwestern China has a significant correlation with IOWPSI ($P < .001$) in the cold season. However, more diverse indexes, e.g., MEI, Niño3.4 SSTA and SOI, influence the variation in the AI in the warm season. The results are consistent with previous studies by Dai et al. (2007) and Li et al. (2016), which illustrate the importance of indexes related to the Atlantic Ocean, Pacific Ocean and Arctic Ocean in the summer water vapor in northwestern China.

To demonstrate the relationship between these indexes ($r > 0.30$) and the AI, we further compared their normalized time series in Fig. 7. Based on these figures, similar shapes of these factors and the AI are shown for multiple time periods (e.g., spring AI with MEI and IOWPSI after 1990, winter AI with IOWPSI during 2000–2015), which further reveal the AI influencing factors. The relationships between IOWPSI and the AI in winter and spring became tighter in recent decades. Due to the accelerating water cycle, more water vapor is transported from the Indian Ocean to northwestern China (Shi et al., 2007). However, the correlations between the indexes and the AI are rather low, which indicates that other factors, such as the North America Subtropical High, the West Pacific Subtropical High and the Index B of the Tibetan Plateau, influence the variability of the AI (Li et al., 2016; Chen et al., 2014). The influence mechanism of these indexes on aridity in northwestern China is complex and requires further research.

4. Conclusions

This detailed analysis of the trends in the annual and seasonal AI time series for the period of 1961–2015 over northwestern China contributed to a better understanding of the regional and seasonal variations of climate change. For the time series of annual and seasonal AIs of 178 stations in northwestern China, we used the MK test to detect significant trends and employed the TSA to assess the magnitudes of the trends. The SQMK method was applied for shift analysis in the AI time series.

The spatial distribution of the dryness/humidity in the study area showed that a hyper-arid climate was in the central part of the study area, and the climate gradually became more humid to the east and to the west. The regionally averaged value of the AI was lowest in spring and highest in summer. The annual AI trends for most of the 117 meteorological stations were positive, and 38 of these stations were significant at the 0.05 level. More than three-fifths of the stations had positive trends in spring, autumn and winter, while almost equal numbers of stations showed positive and negative trends in summer. In addition, of the significant trends, the positive trends were generally

more dominant than were the negative trends. Significant positive trends of the AI were observed in northern Xinjiang in all four seasons, while trends in the east and south of the study area changed with the seasons. Positive trends were more prevalent in hyper-arid, arid and semi-arid stations, while negative trends were more dominant than positive trends in humid and sub-humid stations. Therefore, it is likely that the spatial distribution of the AI in the study area were becoming more homogeneous. For inter-decadal and seasonal AI changes, the summer and autumn AIs were more sensitive to the warming of recent decades. The AIs in winter and spring both presented increasing trends. The results of trend shift analysis have seasonal and spatial differences. The shifts of positive trends were mostly detected in the 1980s and typically became significant in the subsequent decade, while the shifts of significant negative trends were more inconsistent. The correlation analysis indicated that the AI had a significant correlation with IOWPSI in spring and winter and with MEI, Niño3.4 SSTA and SOI in summer and autumn. A better quantitative insight into the mechanisms that affect the AI variations will be helpful for predicting changes in the dryness/humidity in northwestern China. Additionally, the anthropogenic effects of land use and urbanization should be considered in future studies.

Acknowledgements

The work described in this paper was supported by the following projects: National Basic Research Program of China ('973' Program: No. 2012CB956204), National Natural Science Foundation of China (No. 41475104) and Open Fund of Key Laboratory for Preventing and Mitigating Disaster of Qinghai Province (No. QHKF201702). The authors wish to thank the China Meteorological Data Service Center, National Climatic Center and Earth System Research Laboratory for providing the long-term data. We are grateful to the editors and the anonymous reviewers for their valuable comments and suggestions, which significantly improved the quality of the original submission.

References

Allen, R.G., Pereira, L.S., Raes, D., Smith, M., 1998. Crop Evapotranspiration: Guidelines for Computing Crop Water Requirements. Food and Agriculture Organization, Irrigation and Drainage Paper 56. Rome, Italy.
Bao, C., Zou, J., 2018. Analysis of spatiotemporal changes of the human-water relationship using water resources constraint intensity index in Northwest China. Ecol. Indic. 84, 119–129.
Chen, Y., Takeuchi, K., Xu, C., Cheng, Y., Xu, Z., 2006. Regional climate change and its effects on river runoff in the Tarim Basin, China. Hydrol. Process. 20, 2207–2216.
Chen, Y., Deng, H., Li, B., Li, Z., Xu, C., 2014. Abrupt change of temperature and precipitation extremes in the arid region of Northwest China. Quat. Int. 336 (12), 35–43.
Chen, Y., Li, Z., Fan, Y., Wang, H., Deng, H., 2015. Progress and prospects of climate change impacts on hydrology in the arid region of northwest China. Environ. Res. 139, 11–19.
Cook, E.R., Woodhouse, C.A., Eakin, C.M., Meko, D.M., Stahle, D.W., 2004. Long-term aridity changes in the Western United States. Science 306, 1015–1018.
Dai, A., 2011. Drought under global warming: a review. Wiley Interdiscip. Rev. Clim. Chang. 2 (1), 45–65.
Dai, X., Ma, Z., Li, W., Wang, P., 2007. Water-vapor source shift of Xinjiang region during the recent twenty years. Prog. Nat. Sci. 17 (5), 569–575.
Deng, H., Chen, Y., Shi, X., Li, W., Wang, H., Zhang, S., Fang, G., 2014. Dynamics of temperature and precipitation extremes and their spatial variation in the arid region of Northwest China. Atmos. Res. 138 (3), 346–355.
Fu, Q., Feng, S., 2014. Responses of terrestrial aridity to global warming. J. Geophys. Res.-Atmos. 119 (13), 7863–7875.
Gocic, M., Trajkovic, S., 2013. Analysis of changes in meteorological variables using Mann–Kendall and Sen's slope estimator statistical tests in Serbia. Glob. Planet. Change 100, 172–182.
Goossens, C.H., Berger, A., 1986. Annual and seasonal climatic variations over the Northern Hemisphere and Europe during the last century. Ann. Geophys. 4, 385–400.
Hamed, K.H., Rao, A.R., 1998. A modified Mann-Kendall trend test for autocorrelated data. J. Hydrol. 204 (1–4), 182–196.
Han, X., Xue, H., Zhao, C., Lu, D., 2016. The roles of convective and stratiform precipitation in the observed precipitation trends in Northwest China during 1961-2000. Atmos. Res. 169, 139–146.
He, Z., Liang, H., Yang, C., Huang, F., Zeng, X., 2018. Temporal–spatial evolution of the hydrologic drought characteristics of the Karst drainage basins in South China. Int. J. Appl. Earth Obs. Geoinf. 64, 22–30.
Hu, R., Ma, H., Fan, Z., Wu, S., He, W., 2002. The climate trend demonstrated by changes of the lakes in Xinjiang since recent years. J. Arid. L. Resour. Environ. 16 (1), 20–27 (in Chinese).
Hu, Q., Pan, F., Pan, X., Zhang, D., Li, Q., Pan, Z., Wei, Y., 2015. Spatial analysis of climate change in Inner Mongolia during 1961–2012, China. Appl. Geogr. 60, 254–260.
Huang, X., Zhang, M., Jia, W., Wang, S., Zhang, N., 2011. Variations of surface humidity and its influential factors in Northwest China. Adv. Water Sci. 22 (2), 151–159 (in Chinese).
Huo, Z., Dai, X., Feng, S., Kang, S., Huang, G., 2013. Effect of climate change on reference evapotranspiration and aridity index in arid region of China. J. Hydrol. 492, 24–34.
Kendall, M.G., 1975. Rank Correlation Measures. Charles Griffin, London.
Li, B., Chen, Y., Chen, Z., Xiong, H., Lian, L., 2016. Why does precipitation in Northwest China show a significant increasing trend from 1960 to 2010? Atmos. Res. 167, 275–284.
Liu, X., Zhang, D., Luo, Y., Liu, C., 2013. Spatial and temporal changes in aridity index in Northwest China: 1960 to 2010. Theor. Appl. Climatol. 112, 307–316.
Ma, Z., Kang, S., Zhang, L., Tong, L., Su, X., 2008. Analysis of impacts of climate variability and human activity on streamflow for a river basin in arid region of Northwest China. J. Hydrol. 352, 239–249.
Mann, H.B., 1945. Non-parametric tests against trend. Econometrica 13, 245–259.
Nastos, P.T., Politi, N., Kapsomenakis, J., 2013. Spatial and temporal variability of the Aridity Index in Greece. Atmos. Res. 119 (1), 140–152.
Penck, A., 1910. Versuch einer Klimaklassifikation auf physiogeographischer Grundlage. Sitzungsber. Preuss. Akad. Wiss. 12, 236–246.
Salas, J.D., Delleur, J.W., Yevjevich, V., Lane, W.L., 1980. Applied Modelling of Hydrologeic Time Series. Water Resources Publications, Littleton, Colorado.
Salinger, M.J., 2005. Climate variability and change: past, present and future – an overview. Clim. Chang. 70 (1–2), 9–29.
Sayemuzzaman, M., Jha, M.K., 2014. Seasonal and annual precipitation time series trend analysis in North Carolina, United States. Atmos. Res. 137, 183–194.
Schwalm, C.R., Anderegg, W.R.L., Michalak, A.M., Fisher, J.B., Biondi, F., Koch, G., Litvak, M., Ogle, K., Shaw, J.D., Wolf, A., Huntzinger, D.N., Schaefer, K., Cook, R., Wei, Y., Fang, Y., Hayes, D., Huang, M., Jain, A., Tian, H., 2017. Global patterns of drought recovery. Nature 548 (7666), 202–205.
Sen, P.K., 1968. Estimates of the regression coefficient based on Kendall's tau. J. Am. Stat. Assoc. 63 (324), 1379–1389.
Shi, Y., Shen, Y., Kang, E., Li, D., Ding, Y., Zhang, G., Hu, R., 2007. Recent and future climate change in Northwest China. Clim. Chang. 80, 379–393.
Shi, J., Cui, L., Wen, K., Tian, Z., Wei, P., Zhang, B., 2018. Trends in the consecutive days of temperature and precipitation extremes in China during 1961–2015. Environ. Res. 161, 381–391.
Sneyers, R., 1990. On the Statistical Analysis of Series of Observations. WMO. Tech. Note (143). World Meteorological Organization, Geneva, pp. 192.
Some'e, B.S., Ezani, A., Tabari, H., 2012. Spatiotemporal trends and change point of precipitation in Iran. Atmos. Res. 113, 1–12.
Tabari, H., Aghajanloo, M.B., 2013. Temporal pattern of aridity index in Iran with considering precipitation and evapotranspiration trends. Int. J. Climatol. 33 (2), 396–409.
Theil, H., 1950. A rank-invariant method of linear and polynomial regression analysis. Proc. K. Ned. Akad. Wet. 386–392 A53.
Türkes, M., 2003. Spatial and temporal variations in precipitation and aridity index series in Turkey. In: Bölle, H.-J. (Ed.), Mediterranean Climate: Variability and Trends. Springer, Berlin, pp. 181–213.
UNESCO, 1979. Map of the World Distribution of Arid Regions. Explanatory Note, Man and Biosphere (MAB).
von Storch, H., 1995. Misuses of statistical analysis in climate research. In: Storch, H.V., Navarra, A. (Eds.), Analysis of Climate Variability: Applications of Statistical Techniques. Springer, Berlin, pp. 11–26.
Wang, L., Cao, L., Deng, X., Jia, P., Zhang, W., Xu, X., Zhang, K., Zhao, Y., Yan, B., Hu, W., Chen, Y., 2014. Changes in aridity index and reference evapotranspiration over the central and eastern Tibetan Plateau in China during 1960–2012. Quat. Int. 349, 280–286.
Xin, Y., Mao, W., Li, Y., Zhang, X., Lu, G., Bo, L., 2009. Climate division of seasonal precipitation and their changing trend in Xinjiang. J. Desert Res. 29 (5), 948–959 (in Chinese).
Yang, Y., Feng, Z., Huang, H., Lin, Y., 2008. Climate-induced changes in crop water balance during 1960–2001 in Northwest China. Agric. Ecosyst. Environ. 127, 107–118.
Yang, P., Xia, J., Zhang, Y., Hong, S., 2017. Temporal and spatial variations of precipitation in Northwest China during 1960–2013. Atmos. Res. 183, 283–295.
Yao, J., Yang, Q., Liu, Z., Li, C., 2015. Spatio-temporal change of precipitation in arid region of the Northwest China. Acta Ecol. Sin. 35 (17), 5846–5855 (in Chinese).
Yue, S., Wang, C.Y., 2002. Applicability of prewhitening to eliminate the influence of serial correlation on the Mann-Kendall test. Water Resour. Res. 38 (6), 1068.
Yue, S., Pilon, P., Phinney, B., Cavadias, G., 2002. The influence of autocorrelation on the ability to detect trend in hydrological series. Hydrol. Process. 16, 1807–1829.
Zarch, M.A.A., Sivakumar, B., Sharma, A., 2015. Assessment of global aridity change. J. Hydrol. 520, 300–313.
Zhai, P., Zhang, X.B., Wan, H., Pan, X.H., 2005. Trends in total precipitation and frequency of daily precipitation extremes over China. J. Clim. 18, 1096–1108.
Zhang, Q., Singh, V.P., Li, J., Jiang, F., Bai, Y., 2012. Spatio-temporal variations of precipitation extremes in Xinjiang, China. J. Hydrol. 434–4352, 7–18.
Zhang, Y., Cai, W., Chen, Q., Yao, Y., Liu, K., 2015. Analysis of changes in precipitation and drought in Aksu River Basin, Northwest China. Adv. Meteorol. 4, 1–15.
Zhao, Y., Zou, X., Zhang, J., Cao, L., Xu, X., Zhang, K., Zhang, K., Chen, Y., 2014. Spatio-temporal variation of reference evapotranspiration and aridity index in the Loess Plateau Region of China, during 1961–2012. Quat. Int. 349, 196–206.